Statistics and Probability Letters 144 (2019) 44–51

Contents lists available at ScienceDirect

Statistics and Probability Letters

journal homepage: www.elsevier.com/locate/stapro

A Bayesian hierarchical model for multiple imputation of urban spatio-temporal groundwater levels

Kimberly F. Manago [a], Terri S. Hogue [a], Aaron Porter [a], Amanda S. Hering [b,*]

[a] Department of Civil & Environmental Engineering, Colorado School of Mines, Golden, CO, USA
[b] Department of Statistical Science; Baylor University, Waco, TX, USA

ARTICLE INFO

Article history:
Available online 8 August 2018

Keywords:
Bayesian hierarchical model
Multiple imputation
Separable space–time

ABSTRACT

Groundwater levels in urban areas are irregularly sampled and not well understood. Using a separable space–time Bayesian Hierarchical Model, we obtain multiple imputations of the missing values to analyze spatial and temporal groundwater level fluctuations in Los Angeles, CA.

1. Introduction

California recently experienced the most extreme drought on record (Swain et al., 2014). Mandatory statewide restrictions have been implemented, and water allocations have been decreased in many regions, resulting in short and long-term impacts on water supply sources and water supply reliability, especially in cities such as Los Angeles that depend on imported water sources. In Los Angeles, approximately 80% of the water supply comes from imported sources, heavily relying on snowpack in the Sierra Nevada mountains (LADWP, 2010). However, due to the recent drought, there has been a push for increasing reliance on local water supplies, and groundwater is the primary local source in southern California. In Los Angeles, groundwater typically accounts for 11% of water supply, increasing to approximately 30% during drought years.

The increased reliance on local water supply highlights the need for improved understanding of regional groundwater dynamics in order to estimate sustainable groundwater supplies, which can help to prevent negative impacts of overdraft such as land subsidence, increased sea water intrusion, and decreased groundwater storage capacity (Zektser et al., 2005). In fact, California passed its first groundwater legislation, the Sustainable Groundwater Management Act of 2014 that requires groundwater-dependent regions to halt overdraft and bring basins into balanced levels of pumping and recharge. Yet, recharge in urban areas is not well understood as it is complicated by anthropogenic influences such as groundwater pumping, artificial recharge, landscape irrigation, leaking infrastructure, seawater intrusion barriers, and increased impervious surfaces (Lerner, 1990). In urban areas, zero recharge is assumed due to large areas of impervious surface that do not allow water to infiltrate and recharge the groundwater basin. However, in water limited regions where heavy irrigation occurs, this underestimates the amount of recharge.

The need for improved understanding of urban systems is further amplified by the impending risks associated with future climate change. While it is widely agreed that climate change will cause temperature to increase in the future, projections of precipitation are less certain. However, in the southwestern US, winter and spring precipitation is consistently projected to decrease by 2100 (Georgakakos et al., 2014). Additionally, drought in the southwest is expected to become more frequent, intense, and long lasting (Garfin et al., 2014), strengthened by the current drought that already beats previous historical

* Corresponding author.
E-mail address: mandy_hering@baylor.edu (A.S. Hering).

https://doi.org/10.1016/j.spl.2018.07.023
0167-7152/

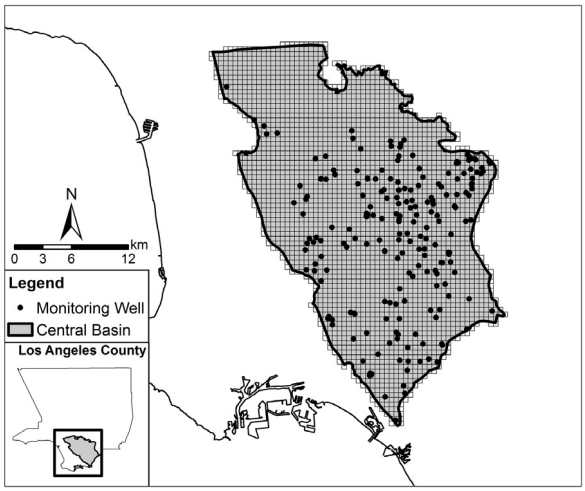

Fig. 1. Central Basin study area and monitoring well locations with 500 m grid used for spatial interpolation.

records. Groundwater is able to provide a flexible buffer during climate-change induced periods of water shortage (Taylor et al., 2013).

Oftentimes, physical groundwater models such as MODFLOW (Langevin et al., 2017) are used to analyze spatial and temporal trends in groundwater levels and recharge. But, many of these models require the estimation of numerous parameters and are prone to both random and systematic model errors (Demissie et al., 2009) that can be difficult to quantify. The launch of the Gravity Recovery and Climate Experiment (GRACE) satellite (Landerer and Swenson, 2012) enables analysis of groundwater levels to be conducted without requiring parameter estimation; however, the spatial resolution is too coarse (300–400 km) to study groundwater fluxes in urban systems. Spatially interpolating observations from groundwater monitoring wells has the potential to solve both of these problems, especially in basins with many wells.

A common problem in using groundwater level data is the irregular sampling of the monitoring wells, resulting in sparsely populated datasets. Thus, imputation is required to provide enough observations to create spatially interpolated maps utilizing methods such as Ordinary Kriging (OK) (Li and Heap, 2011) (and references therein). Bayesian hierarchical models (BHM) have been growing in popularity over the past couple of decades, especially in environmental science (Wikle, 2003) (and references therein). This growth stems from the ability of these models to account for both spatial and temporal effects by factoring their joint multivariate spatio-temporal covariance structures into a series of conditional models. Additionally, they allow for multiple imputation of missing data, a method preferred over single imputation due to the ability to reflect the uncertainty of the missing values in subsequent analyses (Hopke et al., 2001).

The primary goal of this research is to develop a BHM for a set of urban Los Angeles groundwater wells, taking into account both spatial and temporal dependencies, to impute multiple values for each missing groundwater observation. The imputed datasets can then be used to create multiple maps of spatially interpolated groundwater levels at each time step so that the uncertainty of both the missing data and spatial predictions may be estimated. The spatial maps, with their uncertainty estimates, can then be used to analyze spatio-temporal patterns in groundwater levels and to validate hydrologic models. The remainder of this paper is organized as follows: in Section 2, a description of a novel groundwater dataset covering the Central Basin in Los Angeles County is given. The BHM is presented in Section 3. Section 4 analyzes the fit of the model, and we conclude in Section 5.

2. Study area and data

The groundwater basin selected for analysis in this study is the Central Basin, located in Los Angeles County, CA shown in Fig. 1. Los Angeles has a semi-arid, Mediterranean climate, receiving an average of 15 inches of annual precipitation, occurring mainly during the winter months. The Central Basin is one of the primary aquifers supplying water to the Los Angeles Department of Water and Power (LADWP) but also supplies water to nearby cities. In 1965, groundwater in the Central Basin was adjudicated, meaning that all groundwater users in the basin were assigned specific groundwater rights by the courts due to overdrafting that occurred in the early 1960s. To further combat the negative impacts of over-pumping, seawater intrusion barriers were constructed in 1966 and are located in the southern portion of the basin. Additionally, artificial recharge is used to replenish the groundwater reservoir using a combination of imported water sources and runoff.

The groundwater level data used in this study were obtained from the Los Angeles Department of Public Works groundwater monitoring well network (http://dpw.lacounty.gov/general/wells/). The data represent the distance from the ground surface to the water surface in meters; therefore, lower levels indicate that the water is closer to the surface. To make

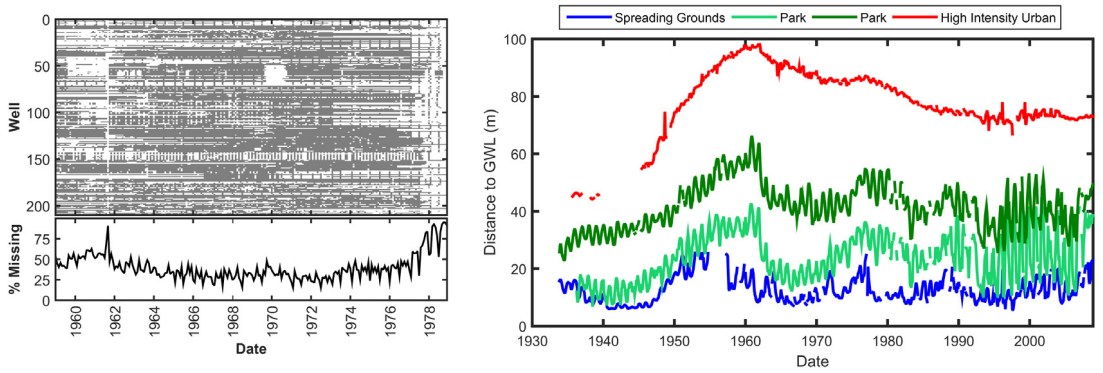

Fig. 2. Exploratory analysis: Temporal coverage of observed data (top-left), where gray indicates observed values and white indicates missing values, and total % of missing data for each time step in the study period 1960–1979 (bottom-left); and historic groundwater level timeseries of select wells with long-term data from 1930 to 2009 (right).

the data more manageable, it was aggregated to a monthly timestep over the 20-year study period from 1960 to 1979, so a total of 240 timesteps are included in the study. The period from 1960 to 1979 is initially selected as a test period because it has the least percentage of missingness, allowing for more rigorous investigation of model performance. Exploratory analysis also showed that this time period experiences the lowest groundwater levels on record followed by a steadily increasing trend. The groundwater data are irregularly sampled with many wells having large temporal gaps between samples, resulting in a sparsely populated dataset, depicted in Fig. 2 (left). Quality control of the data was performed to remove gross outliers, which are potentially the result of input error or measurement error. Additionally, wells with less than 10 observations in the 20-year time period were discarded and not included in the model. This leaves a total of 210 wells that are used in the model (locations shown in Fig. 1), which are missing a mean and median of 39.01% and 33.96% of observations, respectively. This is the first analysis of groundwater levels on this spatial and temporal scale in an urban environment and the first extensive analysis of this particular dataset. The only prior work to use any portion of this dataset was Reichard et al. (2003) who used only 24 monitoring wells to characterize the geohydrologic framework needed for MODFLOW.

Exploratory analysis of the data displays a strong seasonal pattern for some of the wells. Fig. 2 (right) shows four representative wells over the entire time period available where gaps indicate periods of missing values. The three wells showing strong seasonal fluctuations are located in regions near parks and spreading grounds, while the well showing very little seasonal fluctuation is located in an extremely developed region. Seasonal fluctuations are typically caused by seasonality of precipitation, evapotranspiration, and irrigation (Healy and Cook, 2002). In highly developed regions, large areas of impervious surfaces (roads, sidewalks, buildings, etc.) prevent those seasonal factors from influencing groundwater levels as strongly. In general, for all wells, there appears to be an increasing trend in groundwater levels until 1961 at which point, the levels begin to rebound, likely caused by the adjudication of the basin.

3. Methods

One of the primary goals for the groundwater dataset is to create monthly spatial maps of groundwater levels in the region based on observational data. However, due to the high amount of missing data, this is challenging because if missing data are simply ignored, then the number of wells used to create the map in each timestep would change. As a result, the differences between spatial maps could be due to the number and location of the wells used, rather than differences in groundwater levels.

To impute the missing groundwater data, we propose a 4-stage BHM with the following levels:

1. Data Model: [*data* | *spatial process*, *temporal process*, *parameters*]
2. Process Model 1: [*spatial process* | *parameters*]
3. Process Model 2: [*temporal process* | *parameters*]
4. Parameter Model: [*parameters*]

Then, the posterior distribution of the process and parameters updated by the data is:

$$[\textit{spatial process}, \textit{temporal process}, \textit{parameters} \mid \textit{data}] \propto [\textit{data} \mid \textit{spatial process}, \textit{temporal process}, \textit{parameters}] \times [\textit{spatial process} \mid \textit{parameters}] \times [\textit{temporal process} \mid \textit{parameters}] \times [\textit{parameters}]$$

Here, we assume that the spatial and temporal structures are separable conditional on the fixed effects, meaning that for each point in time, the strength and shape of the spatial dependence are the same, and for each spatial location, the strength

and shape of the temporal dependence are the same. This is necessary due to the high percentage of missingness in the data and has the effect of greatly simplifying the model and reducing the variance of the imputed values.

Data model. Let $\mathbf{Z}$ represent groundwater levels at p spatial locations ($p \in \{1, 2, \ldots, 210\}$) and T months ($T \in \{1, 2, \ldots, 240\}$). Thus, $\mathbf{Z}$ is a $(pT) \times 1$ vector ($\mathbf{Z}_{p,T} = [Z_{1,1}, \ldots, Z_{p,1}, Z_{1,2}, \ldots, Z_{p,2}, \ldots, Z_{p,T}]'$). We model $\mathbf{Z}$ as follows:

$$\mathbf{Z} = \mathbf{X}\boldsymbol{\beta} + \mathbf{M}\mathbf{s} + \mathbf{H}\mathbf{u} + \boldsymbol{\epsilon}, \tag{1}$$

where $\mathbf{X}$ is a $(pT) \times 3$ matrix accounting for the intercept and seasonal pattern where each row has the following columns $[1, \sin(2\pi t), \cos(2\pi t)]$, where t is the observation's month, m, converted to radians ($t = m \times \pi/6$); $\boldsymbol{\beta}$ is vector of coefficients of length three corresponding to the model intercept and seasonal harmonics; $\mathbf{M}$ is a known matrix indexing spatial locations; $\mathbf{s}$ is a vector of spatial random effects; $\mathbf{H}$ is a known matrix indexing time; $\mathbf{u}$ is a vector of temporal random effects; and $\boldsymbol{\epsilon}$ is a vector of random errors. The forms of $\mathbf{M}$ and $\mathbf{H}$ can be found in Appendix C. We assume $\boldsymbol{\epsilon} \sim N_{pT}(\mathbf{0}, \sigma_\epsilon^2\mathbf{I})$, with the spatial and temporal process models capturing the dependence in $\mathbf{Z}$.

Process models. The level of missingness makes it very difficult to accurately model the joint covariance matrix of $\mathbf{u}$ and $\mathbf{s}$. Without assuming a separable model, the variance of the imputed values would be too high to produce usable estimates of the missing data. Even with this separable structure, it is important to incorporate model parameterizations that rely on only a few parameters in order to obtain satisfactory model convergence.

Two process models are specified to capture the spatial and temporal processes. The spatial model is defined as $\mathbf{s} \sim N(\mathbf{0}, \boldsymbol{\Sigma}_s(\boldsymbol{\theta}))$, where $\boldsymbol{\Sigma}_s(\boldsymbol{\theta})$ is a spatial covariance matrix with parameters, $\boldsymbol{\theta} = (\sigma_s^2, \theta_s)$, such that: $\boldsymbol{\Sigma}_s(\boldsymbol{\theta})_{p,p'} = \sigma_s^2 e^{-h_{p,p'}/\theta_s}$, where $h_{p,p'}$ is the Euclidean distance between well p and well p'. The spatial model here represents an exponential decay, which is a very flexible, two parameter model. Due to the level of missingness, we also enforce a sum-to-zero constraint on $\mathbf{s}$ to ensure model convergence.

Based on exploratory analysis of each well's partial autocorrelation function, we assume an autoregressive process of order one (AR(1)) for the temporal process. This allows for a short memory process that varies around the seasonal effects in $\mathbf{X}$. The term "short-memory" here refers not to the calendar time of the process, but rather the number of measurements over which the temporal autocorrelation decays. An AR(1) process with a high (low) autocorrelation coefficient can create strong and persistent (weak and short-lived) temporal dependence structure. The AR(1) has the form $u_{p,T} = \alpha u_{p,T-1} + \eta_{p,T}$, where α is the autocorrelation parameter, and $\eta_{p,T}$ is the random temporal deviation at well p and time T. The temporal autocorrelation α is required to lie within the interval $(-1, 1)$ to be stationary. We assume $\eta_{p,T} \sim_{iid} N(0, \sigma_u^2)$, with σ_u^2 unknown, and we enforce a sum-to-zero constraint on $\mathbf{u}$.

Parameter model. All priors are selected to be vague at the scale of the data and conjugate when possible. In the data model, we use a prior of $\boldsymbol{\beta} \sim N_3(\mathbf{0}, \sigma_\beta^2\mathbf{I}_3)$, with a hyperprior of $\sigma_\beta^2 \sim InverseGamma(1, 1)$ ($IG(1, 1)$). We additionally use the prior $\sigma_\epsilon^2 \sim IG(1, 1)$.

The prior distribution for σ_s^2 is chosen as an $IG(1, 1)$. No conjugate prior distribution is possible for θ_s, so it is chosen to be $Unif(0, d)$, where d is selected such that the correlation matrix is effectively one of independence (the largest off-diagonal element in $\boldsymbol{\Sigma}_s(\boldsymbol{\theta})$ is less than 0.001). Uniform weight is placed over this entire domain, so the prior distribution is vague in that sense.

The prior distribution for σ_t^2 is chosen as $IG(1, 1)$. No conjugate prior distribution is possible for the spatial autocorrelation parameter α, so it is selected as $Unif(-1, 1)$, which places equal weight over its entire domain, allowing the prior distribution to be vague. The full conditional distributions resulting from these model specifications are in Appendix A, with the sampling algorithm in Appendix B.

Multiple imputation and spatial prediction. The BHM is used to impute 10,000 values for each missing data point. Then, for a given time step, 1000 maps of predictions are created as follows: if a well is missing for a particular time step, then a random sample of the 10,000 imputations is selected. When a well has observed data for a particular time step, the observed groundwater level is used. Then, Ordinary Kriging (OK) is used to predict groundwater level on a 500 m grid overlaying the domain. This procedure is repeated 1000 times, creating 1000 spatial maps of the groundwater monitoring well data. The prediction uncertainty at each pixel is estimated by calculating the variance of the pixel from the 1000 generated maps, which then includes the uncertainty due to both imputing the missing data and of predicting at new locations.

4. Results and discussion

4.1. Parameters

Visual assessment of the Gibbs chain (see Appendix B) indicates that convergence is met for all parameters within the first 1000 iterations; thus, we discarded the first 1000 iterations and sampled 10,000 subsequent iterations. Based on the posterior distribution of the data, we can analyze the parameter estimates. The spatial covariance parameter, θ_s, has a lower bound of 0 and an upper bound of 1.7 with a mean of 0.77 and standard error of 0.44, indicating weak spatial dependence among wells. On the other hand, the autocorrelation parameter, α ranges from 0.95 to 1, with a mean of 0.99 and standard error of 0.006. The value of α is near the upper boundary, indicating that there is a strong association between observations one month apart. The intercept β_0 has a mean of 32.56 m, similar to the mean of the observed data of 31.83 m. The nonzero estimates of the coefficients, β_1 and β_2, provide evidence that there is a strong harmonic pattern in the data; most likely due to the seasonal pattern of precipitation.

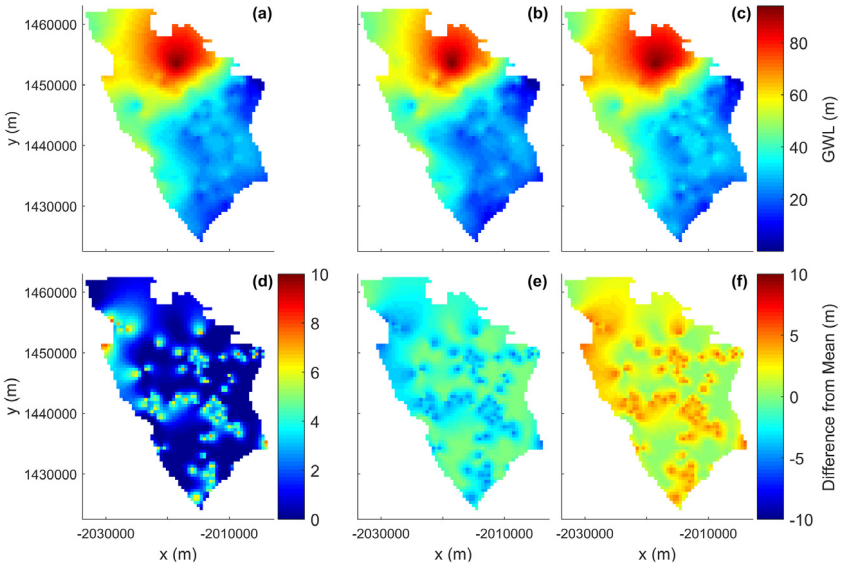

Fig. 3. Spatial maps for July 1974 displaying groundwater levels (m) of the (a) mean of 1000 maps, (b) 2.5 percentile, (c) 97.5 percentile, (d) variance, (e) difference between 2.5 percentile and mean, and (f) difference between 97.5 percentile and mean.

4.2. Spatial predictions

Groundwater level spatial maps are created by calculating the mean of the 1000 OK maps for each timestep. This method allows for the inclusion of all wells in the prediction for each timestep. Thus, discarding wells based on data availability is not necessary, resulting in a smoother change in the maps across timesteps. Since multiple values are imputed for each missing datapoint, spatial maps can be created using the 2.5 percentile and 97.5 percentile of the 1000 OK maps in order to visualize a range of groundwater levels, instead of only producing one map that does not portray the range of values sampled. The lower 2.5 percentile map can be used as a conservative estimate of water levels and to monitor for potential subsidence or overpumping. An additional illustration of how the 1000 OK maps can be used to construct a risk map for monitoring overdraft and recharge is given in Appendix D.

Fig. 3 illustrates one BHM predicted map for July 1974 along with its variance and quantiles. The groundwater maps retain the same overall spatial pattern throughout the twenty year time period, with low water levels in the North-East portion of the basin and water levels increasing towards the South. However, small changes can be seen in localized areas, allowing identification of regions where overpumping or recharge has occurred. The spatial maps of variance provide a quantitative assessment of the areas in the basin with the greatest uncertainty in groundwater levels. This could aid city and regional planners in determining where new monitoring wells need to be installed and can provide confidence in estimates of groundwater availability. In contrast to Fig. 3(d), the OK variance maps produced from the original data only take into account the uncertainty associated with spatial interpolation and do not include the uncertainty associated with imputing the missing data.

4.3. Model fit assessment

Individual timeseries were created for each well to visually assess performance with six examples shown in Fig. 4. Results indicate good model performance. The majority of observed data across all wells is contained within the 95% credible intervals. Only 5.8% of observations fall outside of the 95% credible interval, mainly due to rapid fluctuations in groundwater levels. Overall, the model is able to capture long-term trends in groundwater levels, but in areas with large changes from one month to the next, observed amplitudes are much higher than those predicted by the model. The inability to capture seasonal fluctuations is also apparent in areas where there is little to no fluctuation. This is most likely due to the same seasonal pattern being fit to all wells in the basin.

To illustrate, two pixels are selected, shown in the left panel of Fig. 5. The first is in a 100% highly developed area while the second is located over a spreading ground. These were the land cover classifications that were present in 1960, and they are known to have remained the same throughout the study period. The average absolute changes in the timeseries in the right panel of Fig. 5 are 0.7 m and 1.9 m for the highly developed and the spreading ground pixels, respectively. The highly developed pixel contains mostly impervious surface that does not allow water to permeate and recharge the basin. In the spreading ground pixel, the basin is being intentionally recharged, leading to large fluctuations.

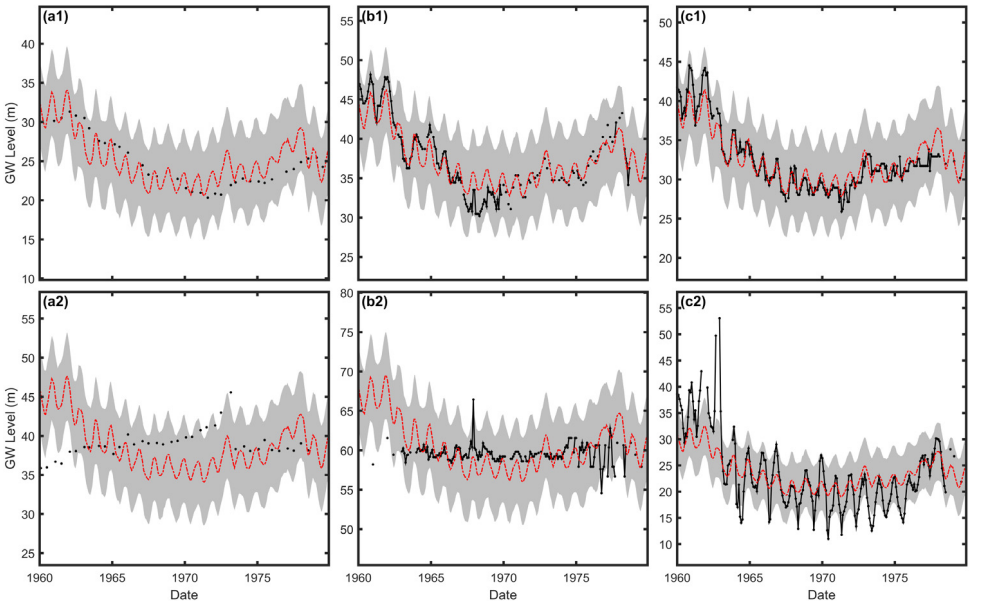

Fig. 4. Wells where the BHM model performed well (top) and poorly (bottom) for comparable amounts of missing data: (a1, a2) 85% missing; (b1, b2) 30% missing; and (c1, c2) 10% missing. The red dashed line is model output, black points are observed data, and gray shaded region is the 95% credible interval.

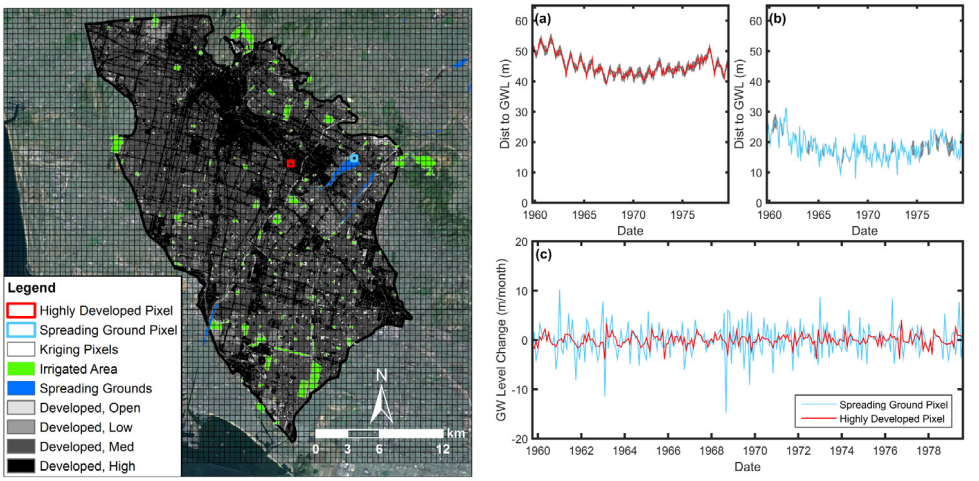

Fig. 5. Grid resolution and land cover map with select pixels for grid comparison (left) and timeseries of groundwater levels for (a) high intensity pixel, (b) spreading ground pixel, and (c) comparison of monthly change $(Z_{p,i+1} - Z_{p,i})$ (right).

Including a land cover covariate in the model could account for the variation in seasonal fluctuations, but such an approach would be difficult to implement. First, land cover in urban areas is extremely diverse, even at the sub-meter scale, making it difficult to assign land cover types to each well. Further, determining the area of land around each well that would influence groundwater fluctuations would be highly dependent on soil parameters that are difficult to obtain or estimate. Second, monthly land cover data from 1960 to 1979 at the 500 m spatial resolution are very difficult to obtain, requiring assumptions that would introduce additional uncertainty to the model. Even if such a covariate were available, some land cover categories have very few wells, which could lead to high variances in the imputed values. Therefore, we simply investigate deviations in model fit by land cover class after fitting the model.

To further investigate, the root mean squared error (RMSE) for each well is computed using $\text{RMSE}(p) = \sqrt{\frac{1}{n_p}\sum_{i=1}^{n_p}(Z_{p,i} - \hat{Z}_{p,i})^2}$, where n_p is the number of observations over time at well p; $Z_{p,i}$ is the observed groundwater level at time i and location p; and $\hat{Z}_{p,i}$ is the corresponding predicted groundwater level. The mean and median RMSE for all modeled wells are 25.1 m and 19.7 m, respectively, while the minimum and maximum RMSE are 2.7 m and 183.0 m,

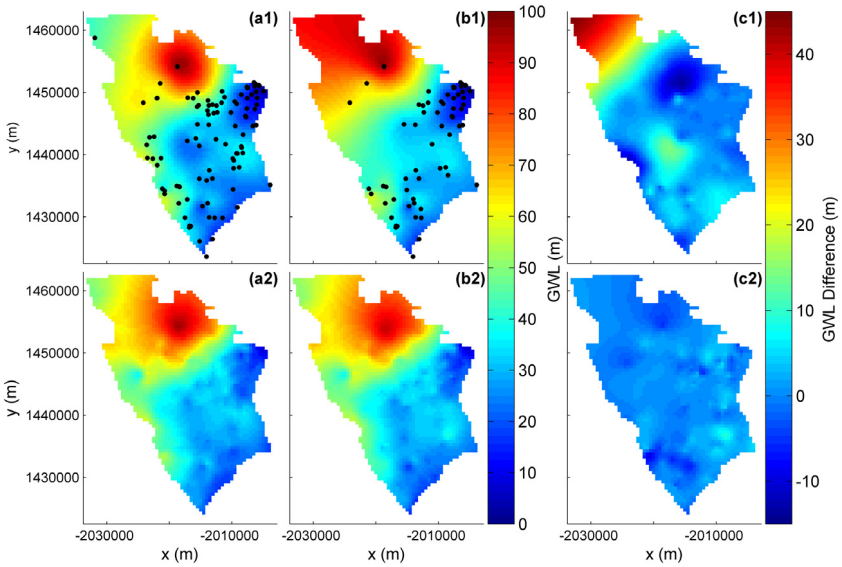

Fig. 6. Spatial maps created using OK applied to the observed data (row 1) and OK applied to the BHM imputed data (row 2) for (a) April 1962, (b) May 1962, and (c) the difference between April 1962 and May 1962.

respectively. The maximum RMSE of 183.0 m is unique to one well, and the next highest RMSE is a much lower value of 88.6 m.

To evaluate the wells with the worst fit, 10% of the wells (21 wells total) with the highest RMSE are selected. Of these, only one well falls within a highly developed area. Four wells are located within an irrigated area, and eleven wells are within 50 m of an irrigated area. These large irrigated areas and spreading grounds were all in existence prior to 1960. In addition, there are two small clusters of four wells and three wells where each well in the cluster is within 500 m of the others. The clustering of wells with high RMSE potentially indicates that the model could benefit from additional screening of wells, based on location, but for this study, no wells were removed due to close proximity.

To evaluate the feasibility of applying the BHM to datasets with a higher percentage of missingness, the model is also applied to the 20-year period from 1980 to 1999, where wells are missing a mean and median of 82.17% and 86.25% of observations, respectively. Similar to the results for the 1960–1979 study period, the majority of observed data across all wells is contained within the 95% credible intervals, with 4.9% of observations falling outside of the 95% credible interval. The mean and median RMSE for all modeled wells are 42.6 m and 26.1 m, respectively. As expected, the RMSE is higher with greater missingness, but it still contains over 95% of observations within the credible intervals.

4.4. Model comparison

Imputing values prior to creating the spatial maps is critical in order to ensure that changes in groundwater level from one time step to the next are due to fluctuations in observed data, not due to the absence or presence of a particular well when using OK applied to the original observations. To illustrate, we create spatial maps using OK applied to the observed data; thus, the number of wells used changes for each timestep based on data availability. The monthly difference between spatial maps is calculated for both the OK spatial maps and the BHM plus OK spatial maps to evaluate the temporal change in groundwater levels between consecutive months; an example is shown in Fig. 6. For the maps created with OK applied to the observed data, it is clear that the changes in groundwater level, especially in the northwest corner of the map, are primarily caused by the presence or absence of wells used for each timestep. The presence of an observation in the northwest corner on April 1962 and its absence in May 1962 results in large changes between the maps created for each month. The monthly change is greater than 40 m in some pixels in the northwest portion of the basin, which is unrealistic. This illustrates the problem with using only observed data to create spatial maps through time, wherein groundwater predictions can be an artifact of the wells used in the spatial interpolation.

In contrast, when comparing monthly changes using OK applied to the BHM imputed dataset, the transitions are much smoother. The mean absolute difference between monthly maps created by OK applied to the observed dataset is 3.82 m (even after removing two large outliers) while it is 1.74 m for the maps created by the BHM imputed dataset. In addition, for the imputed data BHM spatial maps, the general spatial patterns of groundwater levels remain the same with localized areas where larger fluctuations occur. This is much more realistic for groundwater levels and is also useful for finding "hotspots" where overpumping or large volumes of recharge are occurring. Thus, any change between spatial maps is a result of changes in the groundwater levels, not in wells used due to data availability.

5. Conclusion

This study provides a methodology for multiple imputation of missing groundwater level data to create spatial–temporal groundwater level maps. The method allows for estimation of uncertainty in the spatial groundwater level maps caused both by imputing missing data and by predicting at new locations. These spatial maps can then be used to analyze the relationship between groundwater level fluctuations and land cover type. Furthermore, the maps may be used to validate the output of groundwater models, taking into account uncertainty of each pixel. Imputing missing values prior to spatial interpolation leads to realistic temporal transitions between spatial maps. While the dataset in this study primarily utilized historical data from 1960 to 1979, current data being collected from the groundwater monitoring well network could be used to better aid water managers in decision making, and the BHM model could be used to monitor groundwater levels in real time. It could also be used as a predictive model with additional covariates, such as land cover, precipitation, or spreading ground recharge volumes.

Acknowledgments

Kimberly F. Manago and Terri S. Hogue were supported, in part, by the National Science Foundation (NSF) Water Sustainability and Climate Grant (EAR-12040235) and the NSF Engineering Research Center for Reinventing the Nation's Urban Water Infrastructure (ReNUWIt.org; EEC-1028968). Amanda S. Hering was supported by the King Abdullah University of Science and Technology (KAUST) Office of Sponsored Research (OSR) under Award No: OSR-2015-CRG4-2582.

Appendix A. Supplementary data

Supplementary material related to this article can be found online at https://doi.org/10.1016/j.spl.2018.07.023.

References

Demissie, Y.K., Valocchi, A.J., Minsker, B.S., Bailey, B.A., 2009. Integrating a calibrated groundwater flow model with error-correcting data-driven models to improve predictions. J. Hydrol. 364 (3), 257–271.

Garfin, G., Franco, G., Blanco, H., Comrie, A., Gonzalez, P., Piechota, T., Smyth, R., Waskom, R., 2014. Ch. 20: Southwest. In: Climate Change Impacts in the United States: The Third National Climate Assessment. U.S. Global Change Research Program, pp. 462–486.

Georgakakos, A., Fleming, P., Dettinger, M., Peters-Lidard, C., Richmond, T., Reckhow, K., White, K., Yates, D., 2014. Ch. 3: Water Resources. In: Climate Change IMpacts in the United States: The Third National Climate Assessment2. U.S. Global Change Research Program, pp. 69–112.

Healy, R.W., Cook, P.G., 2002. Using groundwater levels to estimate recharge. Hydrogeol. J. 10 (1), 91–109.

Hopke, P.K., Liu, C., Rubin, D.B., 2001. Multiple imputation for multivariate data with missing and below-threshold measurements: Time-series concentrations of pollutants in the Arctic. Biometrics 57 (1), 22–33.

LADWP, , 2010. 2010 Urban Water Management Plan.

Landerer, F.W., Swenson, S.C., 2012. Accuracy of scaled GRACE terrestrial water storage estimates. Water Resour. Res. 48 (4), WO4531.

Langevin, C.D., Hughes, J.D., Banta, E.R., Niswonger, R.G., Panday, S., Provost, A.M., 2017. Documentation for the MODFLOW 6 Groundwater Flow Model. Tech. Rep., In: Techniques and Methods. U.S. Geological Survey, Reston, VA.

Lerner, D.N., 1990. Groundwater recharge in urban areas. Atmos. Environ. B 24 (1), 29–33.

Li, J., Heap, A.D., 2011. A review of comparative studies of spatial interpolation methods in environmental sciences: Performance and impact factors. Ecol. Inform. 6 (3–4), 228–241.

Reichard, B.E.G., Land, M., Crawford, S.M., Johnson, T., Rhett, R., Kulshan, T.V., Ponti, D.J., Halford, K.J., Johnson, T.A., Paybins, K.S., Nishikawa, T., 2003. Simulation-Optimization of the Central and West Coast Basins, Los Angeles County, California. Tech. rep., U.S. Geological Survey, Reston, VA.

Swain, D.L., Tsiang, M., Haugen, M., Singh, D., Charland, A., Rajaratnam, B., Diffenbaugh, N.S., 2014. The extraordinary California drought of 2013/2014: Character, context, and the role of climate change. Bull. Am. Meteorol. Soc. 95 (9), S3–S7.

Taylor, R.G., Scanlon, B., Doll, P., Rodell, M., van Beek, R., Wada, Y., Longuevergne, L., Leblanc, M., Famiglietti, J.S., Edmunds, M., Konikow, L., Green, T.R., Chen, J., Taniguchi, M., Bierkens, M.F.P., MacDonald, A., Fan, Y., Maxwell, R.M., Yechieli, Y., Gurdak, J.J., Allen, D.M., Shamsudduha, M., Hiscock, K., Yeh, P.J.F., Holman, I., Treidel, H., 2013. Ground water and climate change. Nature Clim. Change 3 (4), 322–329.

Wikle, C.K., 2003. Hierarchical models in environmental science. Internat. Statist. Rev. 71 (2), 181–199.

Zektser, S., Loáiciga, H.A., Wolf, J.T., 2005. Environmental impacts of groundwater overdraft: Selected case studies in the southwestern United States. Environ. Geol. 47 (3), 396–404.